JOURNAL OF SOLID STATE CHEMISTRY 89, 167–173 (1990)

Characterization of Copper Cobalt Mixed Oxide

GUO-HUI LI, LI-ZHEN DAI, DA-SHUN LU,* AND SHAO-YI PENG

Institute of Coal Chemistry, Chinese Academy of Sciences, PO Box 165, Taiyuan, Shanxi, 030001, PRC

Received January 12, 1990; in revised form June 8, 1990

Samples of Cu–Co mixed oxide with Cu/Co = 0.25 to 1.0 (atomic ratio) were prepared by coprecipitation with Na_2CO_3 and were characterized with TG, DSC, XRD, and XPS. Exothermic DSC peaks were observed at 588 and 808 K for Cu/Co = 0.25, and at 588, 643, and 683 K for Cu/Co = 1.0. The formation of Cu–Co spinel was observed by XRD after calcination of the samples at 623 K, and increased with prolonged heating at this temperature. But calcination at 773 K for 4 hr destroyed the spinel, producing CuO crystallites. Therefore, Cu–Co spinel is formed above 588 K and is stable at least up to 623 K for Cu–Co ≤ 1.0. The thermal stability of Cu–Co spinel decreases with increasing Cu/Co ratio. The electron binding energies of Cu $2p_{3/2}$, Co $2p_{3/2}$, and O 1*s* are appreciably higher than those in pure CuO and Co_3O_4. This is explanable by the replacement of some Co^{3+} ions at octahedral sites of Co_3O_4 spinel by Cu^{2+}, resulting in a spinel of $Co^{2+}{}_r^{I}Cu_x^{II}Co_{2-x}^{III}O_4^{2-}$, with $r + m + n = x \leq 1$. The locations of Co^{2+}, Cu^{2+}, and Co^{3+} ions in the spinel were inferred from their BE assignments, site preference energies, and the Jahn–Teller stabilization of the octahedral d^9 cupric ion. For samples with a bulk Cu/Co ratio of 0.25, the surface ratio found by XPS is 0.35, while for Cu/Co = 1.0, the surface ratio is 0.55, indicating surface enrichment of Cu–Co spinel. It was also found that the Cu–Co spinel-enriched surface has a lower affinity for oxygen species than that of the pure oxides.

Introduction

Copper–cobalt-based catalysts are versatile in function. Mixed Cu–Co oxides can be used in automobile pollution control (*1*). When promoted by alkali and some other metals, Cu–Co mixed oxide is an excellent catalyst precursor for higher alcohol synthesis from syngas (*2*).

It has been claimed that for higher alcohol synthesis, intimate contact between Cu and Co, or homogeneous distribution of the two metals in the final catalyst, is vital to the success of the catalyst (*3*). Copper–cobalt spinel formation in the precursor is favorable in assuring homogeneity. It has been considered to be present in the IFP precursor without detailed study in this respect (*4*). Mekhandzhiev *et al.* (*1, 5*) had studied the influence of the variation of x in $Cu_x Co_{3-x}O_4$ on catalyst structure and resistance against sulfur poisoning. Yet, studies on this spinel are still very infrequent owing to its instability. Some authors failed to detect any Cu–Co spinel in alcohol synthesis catalysts containing Cu and Co (*6*). Another difficulty lies in the closeness of the XRD patterns of Co_3O_4 and Cu–Co spinels. However, they can still be distinguished by the perceptible displacements.

The present paper presents results of TG, DSC, XRD, and XPS studies on coprecipitated Cu–Co mixed oxides. Special attention is paid to the effect of the Cu/Co ratio

0022-4596/90 $3.00

and calcining temperature on Cu–Co spinel formation and stability.

Experimental

Catalyst Preparation

Solutions of AR grade $Cu(NO_3)_2$ and $Co(NO_3)_2$ were prepared and mixed at Cu/Co ratios of 0.25 to 1.0. The mixtures were precipitated by AR grade Na_2CO_3 solution at 333 K, and the coprecipitates were filtered and washed with deionized water until the filtrate was free from NO_3^-. The catalyst precursors were dried at 393 K for 12 hr, and then calcined at 623 K for 4 hr.

Thermal Analysis

Thermal gravimetry and DSC experiments were carried out on a Dupont 99 thermal analyzer, at a heating rate of 10 K/min, and an air flow rate of 40 ml/min.

X-Ray Diffraction

XRD studies were carried out on a Rigaku Dmax-rA diffractometer using Cu$K\alpha$ radiation and Ni monochromator.

X-Ray Photoelectron Spectroscopy

XPS studies were made with a Perkin–Elmer PHI-5100 instrument, with Al$K\alpha$ radiation of 1486.6 eV as the X-ray source and pass energy of 35.75 eV. The BE scale was calibrated by C 1s = 284.6 eV. The vacuum chamber was pumped to a pressure lower than 10^{-8} Torr.

Results

Thermal Analysis

Results of TG and DSC are shown in Table I and Fig. 1, respectively. Weight loss accompanied by endothermic peaks before 493 K are common for samples with Cu/Co = 0.25 and Cu/Co = 1.0. These might be attributed to evolution of moisture, water of hydration, and CO_2, amounting to about 70% of the total weight loss.

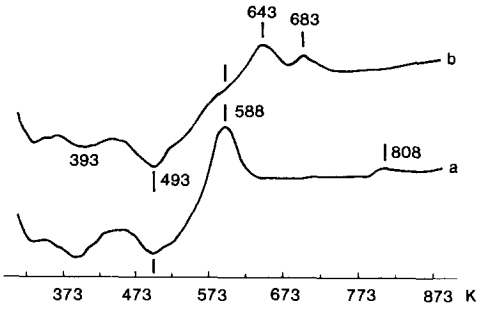

FIG. 1. DSC profiles of coprecipitated precursor curves: a, Cu/Co = 0.25; b, Cu/Co = 1.0.

The Cu/Co = 0.25 sample was characterized by two exothermic peaks at 588 and 808 K, while the Cu/Co = 1.0 sample had exothermic peaks at 643 and 683 K, with only a shoulder at 588 K. These are attached to phase changes mainly, as will be discussed below.

X-Ray Diffraction

XRD patterns of samples with Cu/Co = 0.25 calcined at different temperatures or durations are shown in Fig. 2. Curve a of Fig. 2 is the XRD pattern of a sample calcined at 623 K for 4 h. Spinel structures are incomplete and crystallites are relatively small. Curve b was obtained after the above sample was calcined at 623 K for 12 hr. More complete structures of Cu–Co and Co_3O_4 spinels are observed. The two sets of peaks can be distinguished more clearly, and the 2θ values of the Cu–Co spinel peaks correspond to those of a standard sample described in ASTM Powder Diffraction File as $Cu_{0.3}Co_{0.7}Co_2O_4$ (*7*), which agree also with the data obtained by Angelov *et al.* (*5*) on samples prepared by calcining a stoichiometric mixture of Cu and Co nitrates at 623 K. Curve c was obtained after the above sample was calcined at 773 K for 4 h. Peaks for Cu–Co spinel disappeared, while those

TABLE I

TG RESULTS FOR COPRECIPITATED PRECURSORS

Cu/Co	Temperature range (K)	Peak temperature (K)	Relative weight loss (% of total)	Accumulated weight loss (% of total)	Attributions
0.25	348–448	393	27.8	27.8	Moisture and H_2O of hydration
	448–548	493	44.3	72.1	Decomposition of carbonates
	548–623	588	17.4	89.5	Continued loss of CO_2 and H_2O
	623–723	—	2.6	92.1	
	723–823	808	2.6	94.7	
1.0	348–448	393	21.3	21.3	Moisture and H_2O of hydration
	448–548	493	47.3	68.6	Decomposition of carbonates
	548–623	588	13.4	82.0	Continued loss of CO_2 and H_2O
	623–723	643 683	13.7	95.7	
	723–823	—	3.0	98.7	

for Co_3O_4 spinel remain with sharper shape and are accompanied by clear CuO peaks.

XRD patterns of samples with different Cu/Co ratios but all calcined at 623 K for 4 h, are shown in Fig. 3. Curve c in this figure is the pattern of a sample with Cu/Co = 1.0. Diffraction peaks for Co_3O_4 spinel, Cu–Co spinel, and CuO are observed, with CuO peaks rather strong. Curve b was obtained from a sample with an intermediate Cu/Co ratio of 0.5. Peaks for Cu–Co spinel are hardly distinguishable from those for Co_3O_4, and CuO peaks are weak. Curve a is the same as curve a of Fig. 2.

X-Ray Photoelectron Spectroscopy

Binding energies of Cu $2p_{3/2}$, Co $2p_{3/2}$, and O $1s$ in different samples are summa-

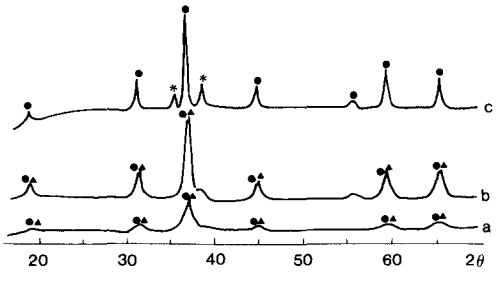

FIG. 2. XRD patterns of Cu–Co oxides, Cu/Co = 0.25. Calcination: a, 623 K, 4 hr; b, 623 K, 12 hr; c, 773 K, 4 hr. Notations: ▲, Cu–Co spinel; ●, Co_3O_4 spinel; *, CuO.

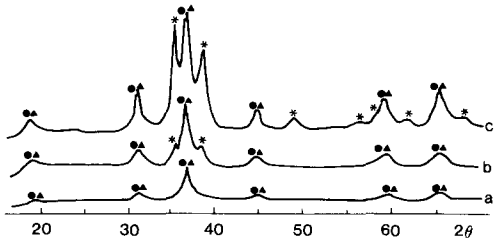

FIG. 3. XRD patterns of Cu–Co oxides calcined at 623 K for 4 hr. Curves: a, Cu/Co = 0.25; b, Cu/Co = 0.5; c, Cu/Co = 1.0. Notations same as in Fig. 2.

TABLE II

XPS RESULTS OF Cu–Co OXIDES

	Literature BE values (eV)	BE in mixed oxides (eV) Cu/Co = 0.25	Cu/Co = 1.0	Attributions
Cu $2p_{3/2}$	933.0 (10)	—	—	CuO
	934.0 (8)	934.0	934.5	Octahedral Cu^{2+}
	936.2 (8)	935.8	936.2	Tetrahedral Cu^{2+}
		941.7	942.7	Satellite
Co $2p_{3/2}$	779.6 (9)	779.6	780.6	Octahedral Co^{3+}
	780.7 (9)	780.3	781.3	Tetrahedral Co^{2+}
	789.5 (9)	790.1	791.1	Satellite
O 1*s*	529.5 (9)	529.8	530.5	Lattice O^{2-}
	530.8 (9)	531.2	532.5	Adsorbed oxygen or OH, CO_3^{2-} etc.

rized in Table II. The original values have been corrected by displacing the energy scale in the direction of literature values (*8–10*) to facilitate comparison. In the cases of Cu 2*p*, Co 2*p*, and O 1*s*, displacements of −5.3, −4.9 and −4.5 eV were made, respectively.

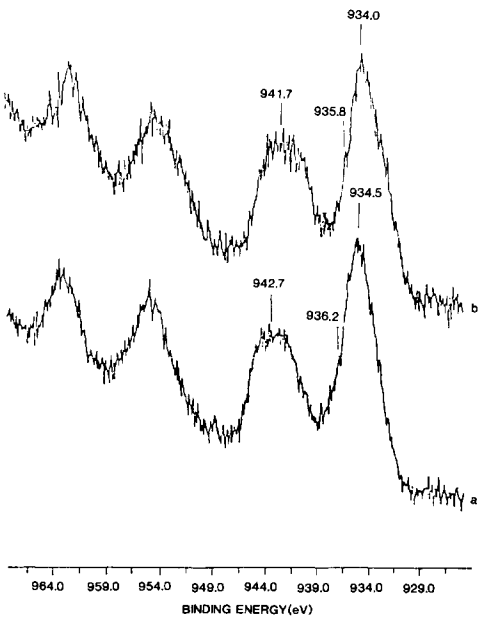

FIG. 4. X-ray photoelectron spectra of Cu $2p_{3/2}$. a, Cu/Co = 1.0; b, Cu/Co = 0.25.

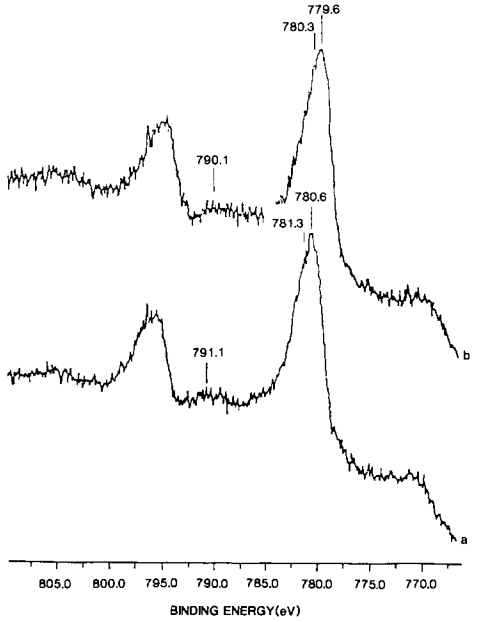

FIG. 5. X-ray photoelectron spectra of Co $2p_{3/2}$. a, Cu/Co = 1.0; b, Cu/Co = 0.25.

Profiles for Cu 2*p*, Co 2*p*, and O 1*s* electron BE's are shown in Figs. 4, 5, and 6, respectively. Obscurities in peak resolution are reduced by comparison with literature and checking with computer deconvolution, so that no conflict should arise from arbitrariness. In Fig. 4, strong satellites indicate divalent Cu (*10*). For Cu/Co = 0.25, the peak at 934 eV can be attributed to octahedral Cu^{2+} in Cu–Co spinel and the 935.8 eV shoulder to tetrahedral Cu^{2+} (*8*). These are appreciably higher than the value 933.0 eV for Cu in pure CuO (*10*). Octahedral Cu is evidently predominant. Quantitative estimation of surface Cu/Co ratio gave a value of 0.35, greater than the bulk value of 0.25.

For Cu/Co = 1.0, BE of Cu $2p_{3/2}$ is about 0.5 eV higher than the corresponding value in Cu/Co = 0.25. From curve a in Fig. 4, the peak at 934.5 eV can be attributed to octahedral Cu, and 936.2 eV to tetrahedral Cu (*8*). The estimated surface

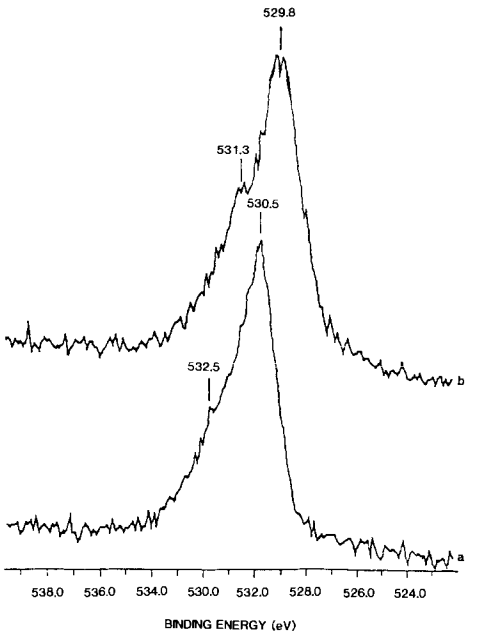

FIG. 6. X-ray photoelectron spectra of O 1*s*. a, Cu/Co = 1.0; b, Cu/Co = 0.25.

Cu/Co ratio is 0.55, much lower than the bulk value 1.0.

In Fig. 5, low intensity satellites indicate that the Co ions are present in the spinel lattice (*9*). For curve b, the attribution of the peaks is 779.6 eV to octahedral Co^{3+}, and 780.3 eV to tetrahedral Co^{2+} (*9*). For curve a, the corresponding values are: 780.6 and 781.3 eV. The BE's for Cu/Co = 1.0 are about 1 eV higher than the corresponding values for Cu/Co = 0.25.

In Fig. 6, O 1*s* BE values for Cu/Co = 0.25 are 529.8 and 531.3 eV. The former may be attributed to lattice oxygen and the latter to surface oxygen, including adsorbed oxygen species and hydroxyl and carbonate groups (*9, 11*). For Cu/Co = 1.0, O 1*s* values are 530.5 and 532.5 eV for lattice and surface oxygens, respectively. Again, a higher Cu/Co ratio gives a higher BE. But the increase of BE with an increasing Cu/Co ratio seems to be only marginally significant, when the reproducibility of measurements is carefully examined.

Discussion

The Formation and Stability of Cu–Co Spinel

Standard XRD profiles for Co_3O_4 and Cu–Co spinel phases given in literature (*7, 12*) show that they are so closely similar that only barely perceptible differences in diffraction from 311, 511, and 111 planes can be observed. The 2θ values at these planes for Co_3O_4 are 36.8, 59.2, and 19.0°, respectively, while those for Cu–Co spinel are 37.0, 59.6, and 19.2°, corresponding to differences in d values of only about 0.01 Å. Therefore the presence of Cu–Co spinel in a matrix of Co_3O_4 can be discerned only by very careful inspection at higher resolution. This might be a reason why many authors failed to detect Cu–Co spinel in Cu–Co mixed oxide. The other cause of missing Cu–Co spinel might be its thermal instability or the relatively narrow temperature range within which it forms and exists, as suggested by the following discussions.

All samples of Cu/Co = 0.25, 0.5, and 1.0 calcined at 623 K gave XRD patterns showing the existence of Cu–Co spinel (Fig. 3). The exothermic peak at 588 K of the DSC curve for Cu/Co = 0.25 and a shoulder at the same temperature in the case of Cu/Co = 1.0 (Fig. 1) can be related to Cu–Co spinel formation. There should be two steps in the formation of Cu–Co spinel: the oxidation of a part of the Co^{2+} to Co^{3+}, and the crystallization leading to the spinel phase. Since no sign of oxygen uptake was detected in the differential TG curves (only numerical values are given in Table I) the oxidation process might have taken place in some earlier stages of preparation, especially in the drying of the precipitate. The remaining possibility contributing to the peak is crystallization, which should also be exothermic. From Fig. 3, it can be deduced that the de-

composition temperature of Cu–Co spinel in all the three samples should be higher than 623 K.

There is no heat change in the DSC curve for Cu/Co = 0.25 beyond 588 K, until a peak appears around 808 K. This may be related to the transformation of Cu–Co spinel into Co_3O_4 spinel and CuO. The calcination of the sample at 773 K for longer periods gave XRD patterns showing no Cu–Co spinel but CuO and Co_3O_4. It is possible that the transformation began at an appreciable rate before the peak temperature.

For the sample with Cu/Co = 1.0, exothermic peaks for the formation and transformation of Cu–Co spinel crowd together at 588, 643, and 683 K. No more peaks appear beyond 683 K. The transformation of Cu–Co spinel into CuO and Co_3O_4 should be completed at this temperature. From this, it is clear that the thermal stability of Cu–Co spinel is dependent on the Cu/Co ratio of the mixed oxide, with lower stability for higher Cu/Co ratio.

The slowness of weight loss beyond 548 K, as shown in Table I, justifies the attribution of the exothermic peaks to phase changes.

Effects of Copper Incorporation in Spinel

The site preference energies, defined as the difference between the CFSE's for octahedral and tetrahedral coordinations of a transitional metal ion, for Co^{3+}, Cu^{2+}, and Co^{2+} are 19.0, 15.2, and 7.4 eV, respectively (*13, 14*). Therefore, it is reasonable for a Cu^{2+} to take an octahedral site occupied originally by a Co^{3+} ion, rather than to take a tetrahedral site occupied by Co^{2+}, as suggested by XPS assignments.

Compared to the stoichiometric formula for spinel, $A^{2+}B_2^{3+}O_4^{2-}$, the Cu–Co spinel unit, $Co^{2+}Cu^{2+}Co^{3+}O_4^{2-}$, will have a surplus electron which must be given off to maintain electrical neutrality. The formula should then be: $Co^{2+r}Cu^{2+m}Co^{3+n}O_4^{2-}$, or more generally, $Co^{2+r}Cu_x^{2+m}Co_{2-x}^{3+n}O_4^{2-}$, where $r + m + n = x \leq 1$. The cations are then more positive than usual, or alternatively, oxygen may be considered as having a valence higher than -2, or less negative than usual. This might be a cause, if not the only cause, of increased BE's observed in Cu–Co mixed oxides. In Table II, Cu $2p_{3/2}$ in the mixed oxides shows the most pronounced effect of increased BE compared to that in pure CuO, while Co $2p$ and O $1s$ have smaller changes, implying that $m \gg r$ and n. This means that Cu^{2+} ions at octahedral sites in Cu–Co spinel carry the most part of the extra charge.

Other important features of the problem are the instability of Cu–Co spinel and its enrichment on the surface. Cupric ion is especially prone to the Jahn-Teller effect (*15*). As a result, the octahedral Cu^{2+} will have its *trans* groups along its z-axis displaced away from the Cu^{2+} center and the planar groups in the x–y plane moving toward it, so that the symmetry is lowered and the degeneracy of $d_{x^2-y^2}$ and d_{z^2} orbitals is removed (*16*). The antibonding orbital resulting from the d_{z^2} is lower in energy than that from the $d_{x^2-y^2}$ orbital, and is therefore occupied. This weakened the Cu–O bond along the z-axis and elongated it. At the same time, the shortening of Cu–O bonds in the x–y plane increases the covalent character of these bonds and contributes to the stability of the distorted octahedron. However, the distorted octahedron is still higher in energy than the Co^{3+} octahedron, and does not conform to the original cobalt spinel lattice. It is then not surprising that the Cu–Co spinel structure containing distorted Cu octahedrons tends to "float" to the surface, making it richer in Cu than the bulk when Cu/Co of the bulk is low, and conversely when the Cu/Co ratio of the bulk is high, as shown in Table III. This is because the stoichiometric Cu/Co ratio of a Cu–Co spinel unit is 0.5. Its enrichment on the surface shall make the surface Cu/Co ratio approach this value from either side.

TABLE III

RATIOS OF ELEMENTS ON SURFACE

Oxides	Cu/Co on surface (atomic ratio)	O/(Cu + Co) on surface (atomic ratio)
CuO	—	2.44
Co_3O_4	—	2.13
Mixed oxide with Cu/Co = 0.25	0.35	1.64
Mixed oxide with Cu/Co = 1.0	0.55	1.45

In Table III, atomic ratios of oxygen to metal are also shown for different samples. For pure CuO and Co_3O_4, the stoichiometric ratios are 1.0 and 1.33, respectively. The stoichiometric O/(Cu + Co) ratio for a Cu–Co spinel unit is also 1.33. The experimental values are much higher, indicating additional oxygen species are present on the surface and not removed by the degassing operation before XPS measurements. Possible forms of these species may include elemental oxygen and combined oxygen in CO_2, H_2O, and OH groups. The decrease in surface oxygen with increasing Cu/Co ratio is interesting because it suggests the lowering of the affinity of the surface for oxygen. This means that Cu–Co spinel adsorbs O species weaker than CuO and Co_3O_4. If the z-axis of the Cu^{2+} octahedron is taken as the direction perpendicular to the surface, then Cu–O bonding shall be weak along this direction as predicted by Jahn-Teller's effect.

Conclusions

1. Copper–cobalt spinel with Cu^{2+} mainly at octahedral sites is formed in mixed Cu–Co oxide when calcined, and tends to concentrate at the surface.

2. The thermal stability of Cu–Co spinel decreases with increasing Cu/Co ratio. With the Cu/Co ratio below 1.0, a calcination temperature of 588–623 K may be recommended for the formation and existence of Cu–Co spinel.

3. The mixed oxide surface enriched with Cu–Co spinel has lower affinity for oxygen species than pure CuO and Co_3O_4 surfaces.

4. The BE of Cu $2p_{3/2}$, and probably also those of Co $2p_{3/2}$ and O $1s$, is raised by the formation of Cu–Co spinel.

Acknowledgments

The present work is supported by the National Natural Science Foundation of China. XPS studies were financed by the United Test Center of Zhong Guan Cun District of Beijing. Mr. Li-Zhu Wen's assistance in experimental work is also gratefully acknowledged.

References

1. G. N. BLIZNAKOV AND D. R. MEKHANDZHIEV, *Kinet. Catal.*, **28,** 100 (1987). [in English]
2. A. SUGIER AND E. FREUND, US Patent 4,122,110, May 11, 1978.
3. P. COURTY AND C. MARCILLY, *in* "Preparation of Catalysts III," (G. Poncelet, P. Grange and P. A. Jacobs, Eds.), p. 485, Elsevier, Amsterdam, (1983).
4. P. COURTY, D. DURAND, E. FREUND, AND A. SUGIER, *J. Mol. Catal.* **17,** 241 (1982).
5. S. ANGELOV, D. R. MEKHANDZHIEV, B. PIPEROV, A. TERLECKI-BARICEVIĆ, D. JOVANOVIĆ, *Appl. Catal.* **16,** 431 (1985).
6. G. R. SHEFFER, R. A. JACOBSON, AND T. S. KING, *J. Catal.* **116,** 95 (1989).
7. ASTM Powder Diffraction File, Card No. 25-270.
8. A. D'HUYSSER, B. LEREBOUS-HANNOYER, M. LENGLET, AND J. P. BONNELLE, *J. Solid State Chem.* **39,** 246 (1981).
9. T. J. CHUANG, C. R. BRUNDLE, AND D. W. RICE, *Surf. Sci.* **59,** 413 (1976).
10. G. SCHÖN, *Surf. Sci.* **35,** 96 (1973).
11. T. H. FLEISCH, R. F. HICKS, AND A. T. BELL, *J. Catal.* **87,** 398 (1984).
12. ASTM Powder Diffraction File, Card No. 9-418.
13. D. S. MCLURE, *J. Phys. Chem. Solids* **3,** 311 (1957).
14. J. D. DINITZ AND L. E. ORGEL, *J. Phys. Chem. Solids* **3,** 318 (1957).
15. C. J. BALLHAUSEN, "Introduction to Ligand Field Theory," p. 193, McGraw-Hill, New York, 1962.
16. M. C. DAY, JR. AND J. SELBIN, "Theoretical Inorganic Chemistry," p. 319, Reinhold, New York, 1962.